Sustainable Energy Technologies and Assessments 52 (2022) 102148

Contents lists available at ScienceDirect

Sustainable Energy Technologies and Assessments

journal homepage: www.elsevier.com/locate/seta

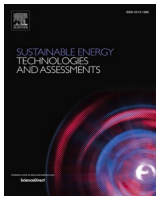

Original article

Multi-objective optimization of a uniformly distributed offshore wind farm considering both economic factors and visual impact

Angel G. Gonzalez-Rodriguez [a,*], Javier Serrano-Gonzalez [b], Manuel Burgos-Payan [b], Jesus Riquelme-Santos [b]

[a] Department of Electric Engineering and Automation, University of Jaen, Campus Las Lagunillas s/n, 23071 Jaen, Spain
[b] School of Industrial Engineering, University of Seville, Av. de los Descubrimientos s/n, 41071 Seville, Spain

ARTICLE INFO

Keywords:
Multi-objective optimization
Offshore wind farms
Visual impact quantification
Power deficit evaluation
Micro-siting
Pareto front
Uniformly-distributed turbines

ABSTRACT

The investment profitability is the strongest economic driver when deciding the location, and optimizing the orientation and layout of a wind power plant. However, and despite of their usual good social acceptance, wind farms must overcome the displeasure of some neighbouring residents, mainly due to the natural landscape alteration. Optimization algorithms must consider the techno-economic aspect, but also the expected visual impact. Unfortunately, there is a lack of objective indicators to quantify it.

Three are the main contributions of this paper. First, it introduces an innovative method of assessing the visual impact of an offshore wind farm, integrated in a optimization algorithm.

Secondly, it explains a method to speed up the annual energy production, allowing the algorithm to optimize the wind farm site and layout within an unlimited space, with unlimited number of turbines, and considering seabed characteristics, depth and cable prices.

Finally, it presents a multi-objective optimization algorithm based on Pareto fronts. With this, a set of optimal solutions has been obtained taking into account the conflicting relationship between profitability and visual impact. The analysis of the optimal solutions also provides the designer with valuable guidelines on the characteristics that the projected wind farm should have.

1. Introduction

The two main aspects in the design of an Offshore Wind Farm (OWF) are economic profitability and environmental impact [1]. The first is determined by the annual flow of income minus expenses once the amortization of the investment and a provision for the estimated decommissioning are discounted. By far, it is the main objective considered by layout optimization algorithms of wind farms.

On the other hand, the environmental impact is a multifaceted factor which is usually a determining aspect of the project success during the planning and acceptance process by the resident population in the neighbourhood.

In that stage, prior to the construction of the OWF, its visual impact (VI) plays a paramount role. Unfortunately, there is not an objective indicator to quantify it.

This work presents an algorithm with a double optimization objective: maximizing the OWF economic profitability and minimizing its VI. The optimization algorithm takes into account this double objective both for the site selection and turbines micro-siting, considering that the optimization of one objective has a negative impact on the other: an exclusively economic analysis often leads to placing the OWF near the coast, where the VI is greater.

1.1. Visual impact

The environmental impact of an OWF involves impact on wildlife (ornithology, marine mammals and resident or migratory fishes), and, if the farm is close to the coast, also noise and VI. There are some other aspects that affect the project social acceptance, as the participation of local communities as co-ownerships of the project, public awareness in favour of clean technologies, or its interference in the path of fishing vessels.

Despite the importance of the VI in the acceptance of an OWF, the assessment of this impact has not been treated from an objective and quantifiable point of view. There is a lack of legislation based on

* Corresponding author.
E-mail addresses: agaspar@ujaen.es (A.G. Gonzalez-Rodriguez), javierserrano@us.es (J. Serrano-Gonzalez), mburgos@us.es (M. Burgos-Payan), jsantos@us.es (J. Riquelme-Santos).

https://doi.org/10.1016/j.seta.2022.102148
Received 3 August 2021; Received in revised form 2 February 2022; Accepted 5 March 2022
Available online 21 March 2022

Glossary

D_{ec}	decommissioning cost
a	annuity factor
inf	annual inflation
r	discount rate
r_i	nominal interest rate
f_l	last front
si	selection index
AEP	annual energy production
CAPEX	capital expenditure
FoV	field of view
IRR	internal rate of return
LCOE	levelized cost of energy
MOOA	multi-objective optimization algorithm
NPV	net present value
nr	number of rows
nt	number of turbines
ntr	number of turbines per row, or columns
OPEX	operational expenditure
SoP	surface of projection
UDPSL	uniformly distributed parallelogram-shape layout
VI	visual impact
WACC	weighted average cost of capital

quantifiable measures of the VI [2] and acceptance of a project is based on park promotion campaigns and surveys on its impact, which in many situations lead to delays or cancellation of the project. Furthermore, these surveys are separated from the iterative design process, and detached from the techno-economic search for the best solution. Only [3,4] provide a VI quantification method agile enough to be included in optimization algorithms, in both cases depending on the horizon occupation and objectifying aesthetic characteristics that favour the deployment of regular arrangements.

In this work, guides to evaluate the OWF VI will be addressed, as one of the optimization objectives.

1.2. Uniformly distributed turbines

Most of academic optimization algorithms [5] use discrete variable for independently locating each of the turbines. The result often leads to irregular arrangement which cannot be standard for engineering practice.

Conversely, different reasons are the cause for evenly distributed wind turbines to be preferentially adopted in most OWFs:

- Symmetrical OWF layouts give rise to appealing VI and reduces maximum turbine loads [1], thus reducing the maintenance cost and increasing the availability.
- From certain institutions, as in New England Wind Energy Area [6], there is an imposition for uniform layouts to address several concerns: navigation safety, creation of distinct transit corridors, and the facilitation of search and rescue operations conducted by vessel and aircraft.
- The land footprint is usually reduced [7].

Optimizations made with and without restricting to uniformly distributed turbines show very small differences in the resulting net energy yield, equal or less than 1% [1,8,9].

On the other hand, optimization methods apply meta-heuristic algorithms that iteratively evaluate massive number of potential solutions. By using traditional or generic methods to evaluate the energy yield, search areas and the turbine numbers are very limited if moderate computation times were expected. Thus, even using simplified methods that lead to errors of up to 10% as in [10], time to complete a search algorithm can exceed one hour for a number of turbines (nt) between 20 and 40. This same author in [11] makes a valuable review of turbine layout studies showing that, except one, all of them limit nt to 60 or less. However, by restricting the configuration to a uniformly distributed parallelogram-shape layout (UDPSL), a drastic reduction of the energy yield evaluation is achieved, thus allowing an unlimited search area and turbine number. It will be discussed in subSection 2.2.1.

1.3. Evaluation multi-objective

Rodrigues in [12] summarized the characteristics of existing approaches to the multi-objective wind farm layout optimization problem. Most of them referred to objectives that were related to techno-economic viability or could even be lumped in a single economic indicator. Tran et al. [13] optimized the energy yield, the necessary area, and the cable length. Mytilinou et al. [14] present the result of twenty-one bi-objective optimizations between seven different technical or economic variables in order to suggest optimum locations for a wind farm. In [15], the annual energy production and the wind farm efficiency are chosen as design objectives.

A search for the optimization of more diverse objectives can be found in [7,16], which introduces, together with an economic objective, the concern for noise reduction.

However, and in the same way that stated in [17], none of the reviewed works incorporated VI in their optimization approaches.

As a new combination of objectives, this paper presents a method that provides the decision maker with a tool to explore the trade-off between the **economic profitability of the investment**, and the project **visual impact**, as an aid to reach the final design. This information is given through a spectrum of possible choices, in which none of them is worse than any other solution for both objective functions. They are known as **non-dominated** solutions and they compose the so-called **Pareto front**. The preferred optimization engines to obtain it are NSGA-II [18] and SPEA-2 [19]. There is an extensive literature comparing the performance of both methods when solving a set of known or particular problems. Although there is not a clear winner among them, it seems that SPEA-2 outperforms NSGA-II in high-dimensional objective spaces, and in general had a better distribution, i.e. less clustering of solutions, specially during the early generations [20]. On the other hand, NSGA-II is faster and superior during latter generations, and was the optimization engine finally chosen.

2. Method

As previously mentioned, in this work a multi-objective optimization algorithm (MOOA) based on Pareto fronts will be developed and its performance will be illustrated by means of a case study. The NSGA-II method has been used. A complete explanation is given in [18], of which the main ideas will be presented in subSection 2.4. It considers two objectives:

Obj. 1. The project viability is determined by the income derived from the sale of energy yield. Rodrigues et al. [12] and Herbert-Acero [17] collected the main indicators of the return on investment in an OWF, describing their advantages and disadvantages. In this work, the levelized cost of energy (LCOE), has been chosen, whose final expression is given in subSection 2.2. Its calculation is enhanced with an exceptionally quick evaluation method of

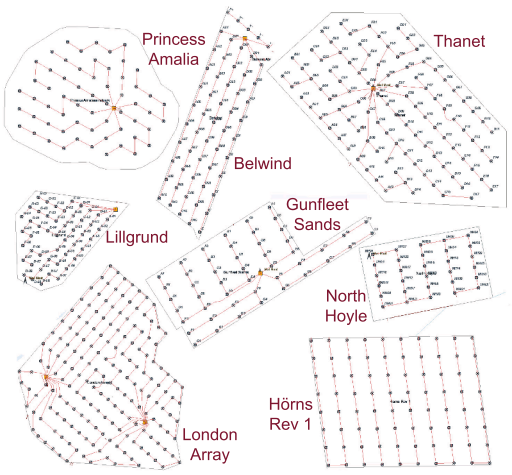

Fig. 1. Actual OWFs with uniform distribution of turbines. Obtained from www.4coffshore.com/offshorewind/.

the annual energy production (AEP), which is described in subSection 2.2.1.

Obj. 2. The OWF VI has been chosen as the second objective. The method to quantify it is given in subSection 2.3.

2.1. Genotype. Definition of the individual

As previously mentioned, several factors favour the uniform distribution of turbines in the OWF. This is the rule of a large number of OWFs today, as seen in Fig. 1. Most papers on layout optimization do not take into account this restriction, which leads to unrealistic solutions while dramatically increasing the decision variable space, to the extent that only a small nt can be investigated in a space of work very reduced and, generally, with the turbines in the centre of a grid of fixed and predefined dimensions.

The decision variable space defining the genotype is reduced if the possible solutions are restricted to UDPSL [21]. This simplifies the genotype to a reduced set of variables, specifically 8, to define possible solutions, as shown in Fig. 2. The variables are:

- Coordinates of the farm centre: $P_c(x_c, y_c)$ $x_c, y_c \in \mathbb{R}$ such that P_c falls within the concession area or search space. In this work, $x_c \in (0\ km, 70\ km)$ and $y_c \in (0km, 24.4km)$.
- Number of rows: $n_r \in \mathbb{N}$
- Number of turbines per row: $n_{tr} \in \mathbb{N}$.
- Distance between turbines along a row: $d_{tr} \in \mathbb{R}^+$
- Distance between rows: $d_r \in \mathbb{R}^+$
- Orientation: $\theta \in [-\pi, \pi]$
- Inclination angle: $\varphi \in (-\pi/2, \pi/2]$

Once defined the individual through these eight parameters, all of the turbine positions can be obtained by geometric operations. Once known these positions, the evaluation of the OWF can be done in terms of profitability or impact, which are the two objective functions. Please note that if any of the turbines falls outside of the concession area, the individual is discarded.

Consequently, the layout optimization problem is transformed into a geometric parameters optimization, providing the designer with meaningful information about the optimal location, orientation and layout of the most suitable OWF designs. Once the dimensions, location and orientation of the parallelogram are obtained, as well as the distance and arrangement of the turbines, the internal structure of the wind farm can be modified in its final design by adding or suppressing individual turbines.

Although not all the OWFs represented in the Fig. 1 correspond exactly to this layout, this genotype constitutes the most realistic approach to site determination within a large concession area.

2.2. Economic evaluation. LCOE as objective 1

The levelized cost of energy (LCOE) is one of the most preferred economic functions to evaluate the profitability of a prospective investment over time. Compared to the net present value (NPV), the former can be used as a measurement of the operation risk and the investment quality. Another reason in its favour compared to NPV or the internal rate of return (IRR), is that NPV and IRR are highly variable from one country to another, impeding the comparison between existing projects around the world. In addition, these indicators require information on the energy price, and in periods in which this price is very volatile, due to, for example, fluctuations in the price of gas, LCOE may be the only valid indicator to evaluate the investment quality.

LCOE can be calculated from:

$$\mathrm{LCOE} = \frac{(CAPEX + Dec)/a + OPEX}{AEP}. \tag{1}$$

where CAPEX is the total investment cost, D_{ec} is the discounted decommissioning cost after deducing the residual price of the plant, OPEX is the operation and maintenance cost, AEP is the annual net energy production (after discounting the total losses due to wake interferences and in the electrical infrastructure), and a is the annuity factor that can be defined as

$$a = \sum_{k=1}^{T} \frac{1}{(1+r)^k} = \frac{1 - \frac{1}{(1+r)^T}}{r} \tag{2}$$

where T is the utility life-time, and r is the discount rate (similar to the weighted average cost of capital (WACC) [22]), which is obtained from the nominal interest rate r_i and the inflation inf as

$$r = \frac{1 + r_i}{1 + inf} - 1. \tag{3}$$

LCOE evaluation requires the knowledge of a numerous set of costs,

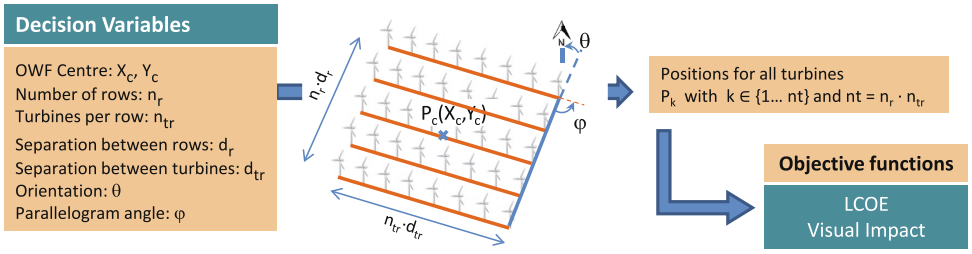

Fig. 2. Parameters defining an individual. Eight parameters define the position for all of the OWF turbines. Once obtained the turbine positions, the objective functions can be evaluated.

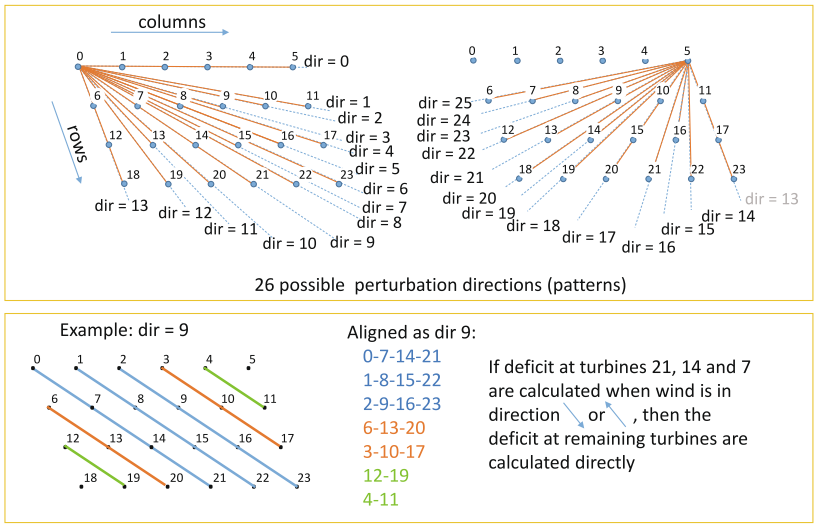

Fig. 3. Perturbation patterns for a uniformly distributed 6x4 layout. The deficit for all of the sequences of turbines along a perturbation pattern is the same and has to be calculated only once.

Table 1
Computation cost for the evaluation of the AEP of some evenly distributed OWF with rhomboidal-shape.

Case	Rows	Turbines per row	Total turbines	Time t(ms)
1	9	7	63	1.9
2	9	12	108	2.5
3	13	13	169	2.6
4	18	12	216	2.1
5	18	22	396	3.34
6	34	22	748	4.3
7	34	30	1020	5.43

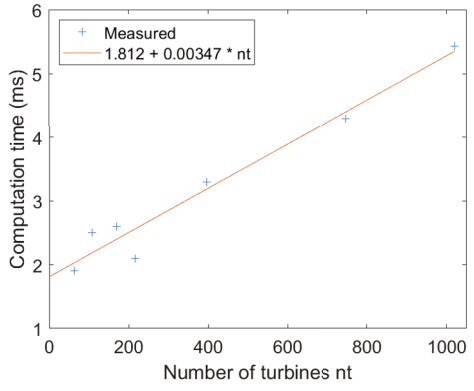

Fig. 4. Time to compute the energy yield as a function of nt.

prices and data, which for the test cases of Section 3, are gathered in Appendix A, and have also been published in [23,24]. Most of them are fixed once decided the number of turbines, the model and the concession zone location. However, the specific turbine positions, as calculated from the eight individual parameters, will modify both the CAPEX (influencing the foundation costs and the cable acquisition/installation costs) and the AEP and therefore determine LCOE.

2.2.1. Innovative calculation of energy yield exploiting UDPSLs

Among the different components of (1), the evaluation of the AEP is the most time-consuming task, since it requires the calculation of actual wind speed at each turbine taking into account the wake losses. Accordingly, an extremely fast method to calculate the AEP is essential to develope and tune optimization algorithms, mainly when a second objective is entered in the exploration of the solution space.

The proposed method, as used in this work, is based on the traditional Park's shadow model, which is the preferred one among the different approaches to the calculation of the energy yield [25]. Formulae and a brief description of this model can be found in [22]. Its key difference with respect to the traditional way of evaluation is based on exploiting the symmetry and repeatability of UDPSLs. This restriction limits the number of possible perturbation patterns to a very reduced value. For example, for an OWF with twenty-four turbines disposed in four arrays, as in Fig. 3, there are twenty-six possible perturbation patterns.

With this procedure, it is necessary to calculate the deficit of the energy yield for the turbines aligned according to all of the patterns. Considering, as an example, the direction 9 (see example of Fig. 3), we have to calculate the energy deficit of the sequence composed by turbines 0-7-14-21. This energy deficit will be the same that for turbines 1-8-15-22 and 2-9-16-23. Furthermore, the energy deficits for the 3-tuples 6-13-20 and 3-10-17, as well as for the 2-tuples 12-19 and 4-11 are also calculated in a straightforward way when analysing pattern 9. This way, by taking into advantage of the calculations to obtain the energy deficit at turbine 21 (last turbine of first 4-tuple) when the incoming wind is in the direction 9, it is possible to obtain the energy deficits at turbines 14, 7 (first 4-tuple), 22, 15, 8 (second 4-tuple), 23, 16, 9 (third 4-tuple), 20, 13 (first 3-tuple), 17, 10 (second 3-tuple), 19 (first duple) and 11 (second duple). This results in a drastic reduction of calculations, reduction that increases with the OWF size.

For all of the patterns, the produced energy (or more exactly, the energy deficits) must be calculated, not only for the incoming wind direction that exactly matches the alignment, but also for wind directions deviated some degrees from the alignment direction. And logically, the calculations must also be performed for all of the incoming wind speeds between the cut-in speed and the cut-out speed.

Keeping an uniform separation between turbines entails a computational simplification; hence, time to evaluate the wind deficits due to wake losses can be dramatically reduced, leading to computation times of few ms per layout evaluation even for very large OWFs. This way, nt is not a limiting aspect in the analysis of OWFs, and does not necessarily increase the computation time, on the contrary that happens with all of the existing optimization algorithms found in the literature, where the computational cost depended on nt^2. The code in Matlab to obtain the annual energy production, both with this fast method and also with the generic one have been published in [26].

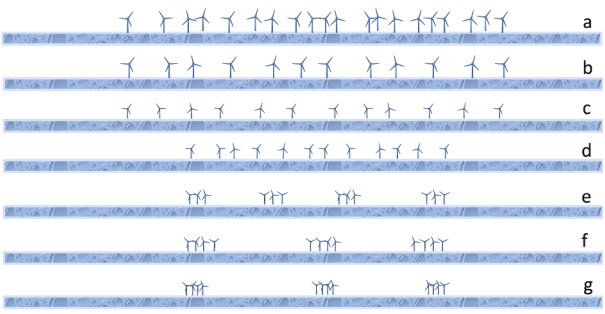

Fig. 5. Factors affecting the Visual Impact.

As an example, Table 1 summarizes the CPU time in a domestic PC (Intel i5-6500 3.2Ghz) corresponding to the evaluation of the AEP of some evenly distributed OWFs with rhomboidal-shape. In all cases, the resulting error is lower than 0.3% with respect to a general wake calculation using Park model [25]. For the calculation of the energy yield, a discretization of 1 deg has been used for the direction of the incoming wind and 1 m/s for its speed.

Fig. 4 shows the growing of the computer time to calculate the AEP with nt. This figure also shows that the relationship between the computer times and nt is well described using the linear regression line:

$$t(nt) \simeq 0.0035 \cdot nt + 1.8179 \qquad R^2 = 0.9588. \tag{4}$$

As seen from the figure, the computation time is rather less than proportional to the turbine number. As for comparison, Wagner et al. [27] indicates a value of 30 s (5500 times higher than the obtained with the proposed method) for 1000 turbines. A value of 90 h for 1 million fitness evaluations for a 169-turbine layout was given by Rodrigues, Bauer and Bosman [15], which means 324 ms per evaluation (124 times higher).

Finally, it is worth mentioning that this method can be used, not only with the Park's model, but with any wake model.

2.3. Visual impact as objective 2

The second objective of the proposed optimization algorithm is the visual impact, which logically must be dynamically quantified along the execution of the search algorithm. Clearly, the main action to be taken to reduce visual impact consists in moving the OWF away from the coast, but if this is not possible (for example because the concession area is fixed or the foundation costs increase), then the developer can take other actions to reduce VI.

2.3.1. Factors affecting the visual impact

A novel indicator is introduced that takes into account the farm visibility in terms of occupancy of the field of view (FoV). This indicator reflects the following causes of visual impact increase (see Fig. 5):

- If turbines occupy more space of the FoV, then VI increases. This can be due to:
  - a larger number of turbines, and thus $VI(a) > VI(b)$
  - larger turbines (or closer to the coast), and thus $VI(b) > VI(c)$
  - more separated turbines, and thus $VI(c) > VI(d)$
- If turbines, as perceived from the observer, are distributed along the wind farm projection, then its visual impact is greater than if gaps appear in the farm silhouette. Therefore $VI(d) > VI(e)$, and the VI is more reduced as bigger the gaps $VI(e) > VI(f)$
- If turbines are aligned along the view direction, the visual impact decreases, and thus $VI(f) > VI(g)$

The aim of this subsection is to describe the expressions that, starting from the turbine positions and its characteristics (height and diameter), as well as the observer position, obtain an indicator of the visual impact perceived by the observer. Fig. 6 can be used as a guide that anticipates the expressions to be used in order to yield intermediate results and to finally obtain the VI. The script in Matlab codifying this VI quantification has been published in [28].

2.3.2. Dimensions of the observer's FoV

The visibility of an OWF, calculated as the occupation of the FoV, is caused by the presence of its turbines in the observer's FoV, which is restricted to 120 deg in the horizontal direction [29,30] and 40 deg in the vertical direction [31]. These values are not widely accepted and the former can be reduced if it is only considered the central FoV [32] or increased if we include the possibility of moving the eyes, or turning the head. In order to quantify the turbines presence, it is necessary to project the FoV and the turbines contained in it onto the so-called surface of projection (SoP), whose dimensions are given by

$$\begin{aligned} x_{FoV} &= d_{SoP}\, 120\pi/180 \\ z_{FoV} &= d_{SoP}\, 40\pi/180 \end{aligned} \tag{5}$$

where d_{SoP} is the distance to the SoP. It entails a drawing scale, and it can be demonstrated that is meaningless for the visibility calculation; hence a value of 1 m can be taken.

Together with the calculation of VI, the following expressions can be used to confection a photo-montage to anticipate the designer or the public with the horizon modification when the OWF is finished. In this case, the value of d_{SoP} can be varied to modify the drawing scale.

Next subsections will analyse how each of the turbines is projected

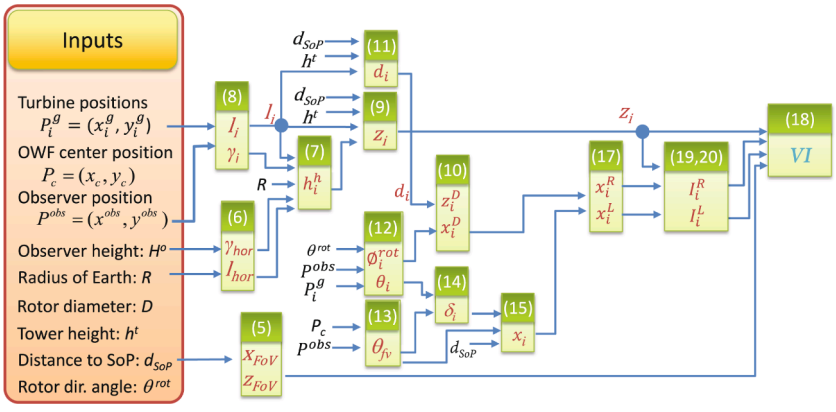

Fig. 6. Stream of calculations to obtain the visual impact. Input variables are written in black and intermediate variables, in brown. The expressions linking the variables appear in white.

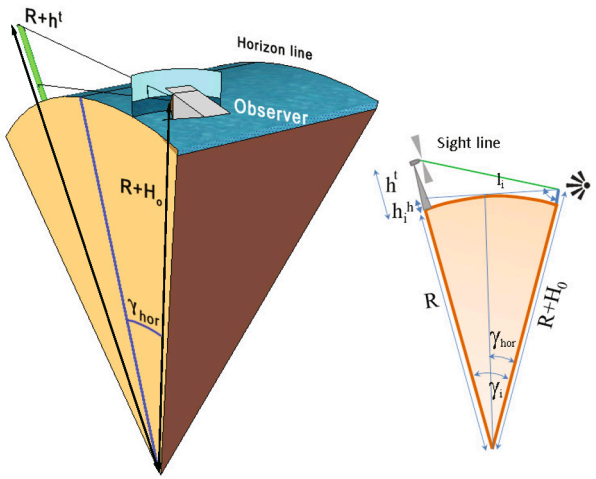

Fig. 7. Representation of distances and angles between observer, horizon line and turbine.

onto the SoP, and expressions will be provided to calculate the dimensions and position of its projections.

2.3.3. Visible part projection of tower for turbine i

Due to the Earth curvature, part of the tower basis can be hidden by the horizon line if the turbine is located beyond the horizon distance l_{hor} (see Fig. 7):

$$l_{hor} = R\,\gamma_{hor} \;\text{ with }\; \gamma_{hor} = \arccos\left(\frac{R}{R+H_o}\right) \tag{6}$$

where $R = 6.3710{\cdot}10^6\ m$ is the average Earth radius and H_o is the observer height. The hidden part h_i^h of the tower of turbine i, located at a distance l_i from the viewpoint, is

$$\begin{aligned} h_i^h &= \frac{R}{\cos(\gamma_i - \gamma_{hor})} - R \quad \text{if} \quad l_i > l_{hor} \\ h_i^h &= 0 \quad \text{if} \quad l_i \leqslant l_{hor} \end{aligned} \tag{7}$$

with

$$\begin{aligned} l_i &= \sqrt{(x_i^g - x_{obs}) + (y_i^g - y_{obs})} \\ \gamma_i &= \frac{l_i}{R} \end{aligned} \tag{8}$$

This way, the length of the visible part projection z is

$$z_i = \left(h^t - h_i^h\right)\frac{d_{SoP}}{l_i} \tag{9}$$

where h^t is the tower height.

2.3.4. Rotor projection for turbine i

The rotor surface will be projected onto the SoP as an ellipse with axes

$$\begin{aligned} z_i^D &= d_i \\ x_i^D &= d_i \cos\phi_i^{rot} \end{aligned} \tag{10}$$

with

$$d_i = D\frac{d_{SoP}}{l_i} \tag{11}$$

and

$$\begin{aligned} \phi_i^{rot} &= \theta^{rot} - \theta_i \\ \theta_i &= \arctan\frac{x_i^g - x_{obs}}{y_i^g - y_{obs}} \end{aligned} \tag{12}$$

where D is the rotor diameter, $(x_i^g,\, y_i^g)$ and $(x_{obs},\, y_{obs})$ are the geographical coordinates of the i-turbine and observer, respectively, and θ^{rot} is the direction angle of the rotor, which in normal operation matches the wind direction.

2.3.5. Separation between turbine projections

In order to determinate the horizontal positions of the turbine projections, we have to establish the *Frontal View Direction* θ_{fv}, defined as the prevalent direction in which the potential observer looks at the sea. It depends on the observation point characteristics, but if no specifications are given, we can use a perpendicular to the coast or a segment linking the OWF centre and the observer, with angle

$$\theta_{fv} = \arctan\frac{x_c - x_{obs}}{y_c - y_{obs}} \tag{13}$$

where $(x_c,\, y_c)$ is the position of the OWF centre. The deviation respect to this direction at which the observer sees the turbine i is obtained from (12) and

$$\delta_i = \theta_i - \theta_{fv} \tag{14}$$

Having in mind that SoP is a cylindrical surface, not a planar one, then the x-coordinate of tower i projection is

$$x_i = d_{SoP}\delta_i = d_{SoP}(\theta_i - \theta_{fv}) \tag{15}$$

Without lose of generality, we can consider that x_i are sorted in ascending order.

$$-x_{FoV}/2 < x_1 < \ldots < x_j < x_{j+1} < \ldots < x_{nt} < x_{FoV}/2 \tag{16}$$

Otherwise, they must be sorted as shown in Fig. 8. This figure also represents, in a simplified way, the merged occupation of FoV by overlapping the rectangles bounding the turbines. In this figure, the left and right edges of the enveloping rectangle are calculated from (10):

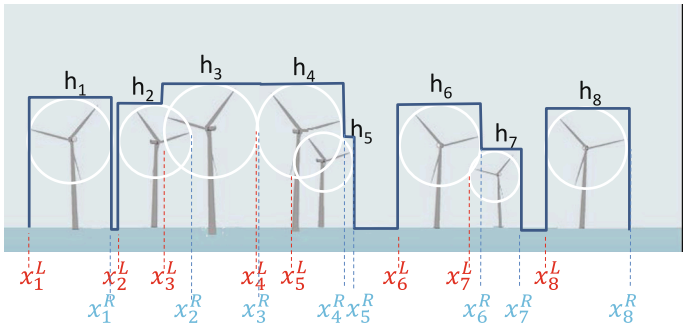

Fig. 8. Disposition of the turbine projections onto the straightened picture surface, and overlapped representation of the turbines by mean of rectangles.

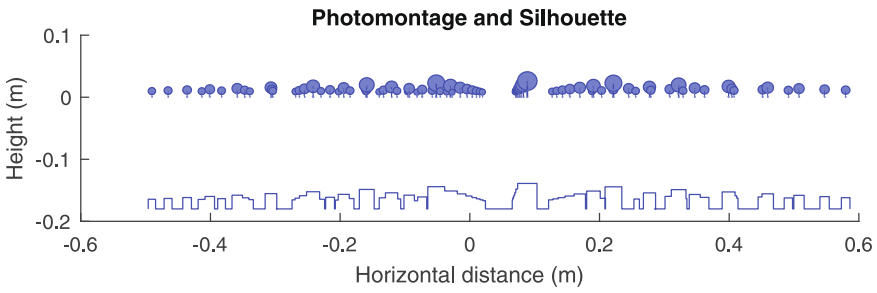

Fig. 9. Representation of the turbines along the horizon line and merged occupation of the FoV. A distance to canvas equal to one has been used for the representation.

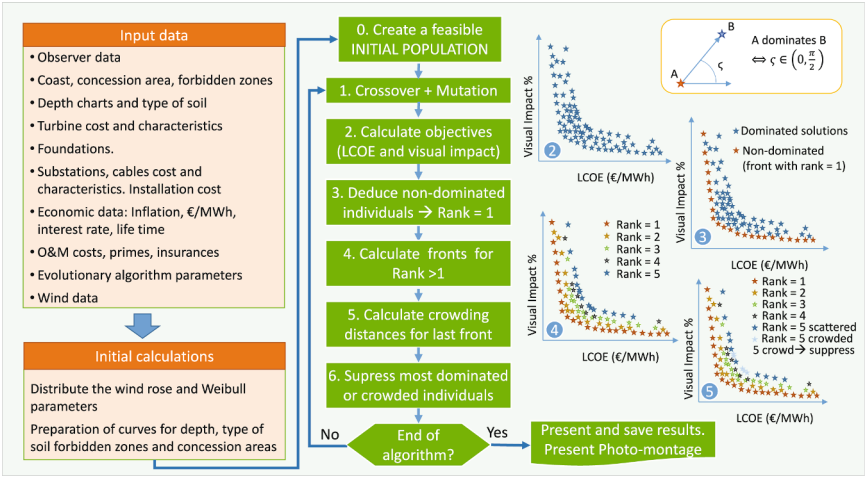

Fig. 10. Flowchart of the NSGA II algorithm for optimizing LCOE and VI of an OWF.

$$x_i^L = x_i - x_i^D/2 \text{ and } x_i^R = x_i + x_i^D/2 \tag{17}$$

2.3.6. Visual Impact as the Merged Occupation of the FoV

Certain issues such as the size of the turbines and distance, their overlapping or the rotor orientation, determine the visibility V of an OWF from a viewpoint. It is calculated as the fraction of the FoV that is occupied by the projection of the turbines, taking into account the overlapping as in Fig. 8.

$$VI = \frac{\sum_{i=1}^{nt}(I_i^R - I_i^L)\cdot z_i}{x_{FoV} z_{FoV}} \tag{18}$$

where L and R stand for left and right, and

$$I_i^R = \min(x_i^R, \min(x_j^L)) \quad \text{with} \begin{cases} j \neq i \\ z_j > z_i \\ x_i^L < x_j^L < x_i^R \end{cases} \tag{19}$$

$$I_i^L = \max(x_i^L, \max(x_j^R)) \quad \text{with} \begin{cases} j \neq i \\ z_j > z_i \\ x_i^L < x_j^R < x_i^R \end{cases} \tag{20}$$

For a more accurate evaluation, the wind rose must be taken into account because the rotor orientation, and consequently its visibility, depends on the direction of the incoming wind via (17) and (10). Therefore, the impacts for each of the orientations given by the wind rose must be calculated and weighted averaged (See Fig. 9).

2.4. Pareto front

The final objective of this work is to offer a set of non-dominated solutions that allow the choice of the best location, and eventually, the optimal arrangement of the turbines with two objectives: a high return of investment measured as a low LCOE; and low VI, so that it does not produce rejection in the resident population. Therefore, LCOE and VI conform the objective functions space.

The key concept at MOOA is the dominance relationship. As previously introduced, and assuming that all objective functions must be minimized, a solution **A** dominates another **B** if all the objective functions of **A** are less than or equal to those of **B**, and strictly less in at least one of them. As shown in the upper right corner of Fig. 10, in a graph representing the objective functions, **A** would be below and to the left of **B**. Accordingly, a solution **A** is non-dominated, if there is not a solution **C** dominating **A**.

$$\mathbf{A} \quad \text{non} - \text{dominated} \leftrightarrow \ \neq \ xists\mathbf{C} : \begin{cases} VI(\mathbf{C}) < VI(\mathbf{A}) \quad \& \\ LCOE(\mathbf{C}) < LCOE(\mathbf{A}) \end{cases} \tag{21}$$

This concept is visualized at the upper-right corner of Fig. 10, in which a solution A dominates another solution B, if both VI and LCOE are better (i.e. lower) for the solution A than for the solution B (to be precise, one of the objective function can be lower or equal). In the VI-LCOE plot this means that A is below and at the left respect to B.

In this work, the method NSGA-II has been used to obtain generations with distributed solutions along the Pareto front, exploring the trade-off between these confronting objectives:

- LCOE, as given from (1), whose value must be as low as possible,
- VI, as given from (18), whose value must be also as low as possible,

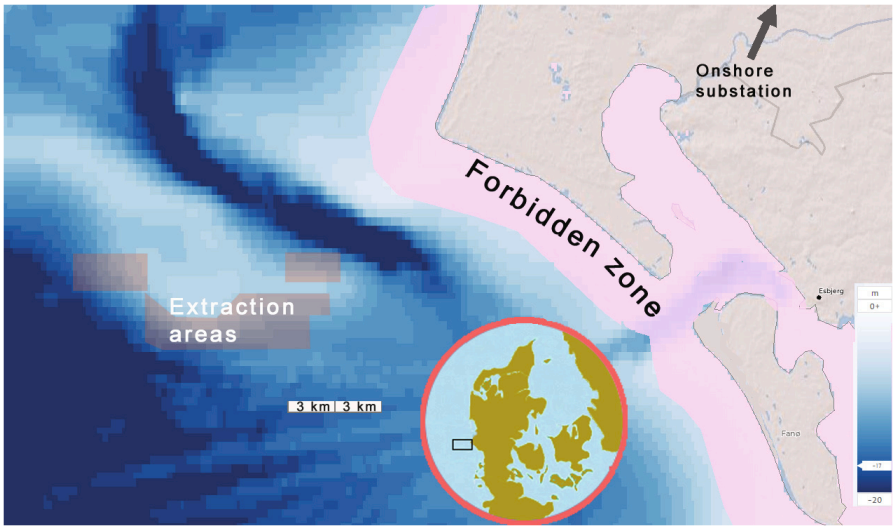

Fig. 11. Map of Horns Rev I site, used as a framework with dimensions 70 km × 27 km. Background of the image obtained from globalwindatlas.info.

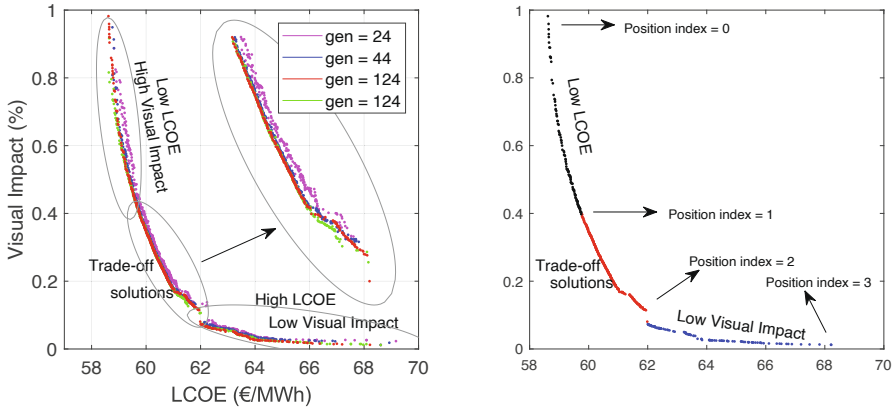

Fig. 12. Evolution of the fronts using NSGA II technique and division into three zones (left-hand plot); final Pareto front using colours to visualize the three zones (right-hand plot).

A flow chart of the NSGA-II is shown in Fig. 10, and a description of the algorithm is given below. A more detailed explanation of this method can be found in [18].

1. An initial population is created with feasible individuals, i.e. individual without turbines outside the concession area (or inside forbidden zones). This will also be the population size of each generation *ps*.
2. New individuals are incorporated by crossing and mutating the existing ones. These new individuals are known as **offspring**.
3. Calculate the LCOE and VI for each individual, which are the two objectives to optimize.
4. Deduce the non-dominated solutions. These are the solutions for which there are no better individuals for both criteria (LCOE and VI). Non-dominated solutions conform the front with rank 1 (see Fig. 10).
5. Deduce the solutions with rank = 2 and successive ones. There is a front of solutions for each rank. A solution belongs to the front with a certain rank if it fulfils two conditions: at least one individual with immediately lower rank is better for both objectives; and is not dominated by any other individual from this front. As the fronts of each rank are calculated, a new generation is created incorporating the individuals of the successive fronts, until, for a certain front, the accumulated number of individuals is greater than or equal to *ps*. This will be the last front (f_l) of the offspring.
6. If the accumulated number of individuals is greater than *ps*, only the more scattered individuals of this front f_l will be incorporated to the new generation. A metric for the dispersion of elements in this front is given by the **crowding distance**, calculated in the objective function space with the aim of distributing the set of solution along the front. Assuming that this front f_l consists of $N(fl)$ individuals, sorted increasingly according to one of the objectives, e.g. LCOE, then the crowding distance is defined as

$$cd_i = \frac{LCOE_{i+1} - LCOE_{i-1}}{LCOE_{N(fl)} - LCOE_1} + \frac{VI_{i+1} - VI_{i-1}}{VI_{N(fl)} - VI_1} \quad 1 < i < N(fl) \tag{22}$$

$$cd_1 = cd_{N(fl)} = +\infty \tag{23}$$

7. For this front -*fl*, suppress the solutions with lower crowding distance *cd* to keep a new generation with *ps* individuals. Also suppress the remaining fronts $f > f_l$..
8. If the number of iterations has been completed (150 for this work), present the results. Otherwise, go back to 2 to create a new offspring.

3. Analyzed case and results

To demonstrate the algorithm performance, it has been used to optimize the OWF location and layout assuming an available area that

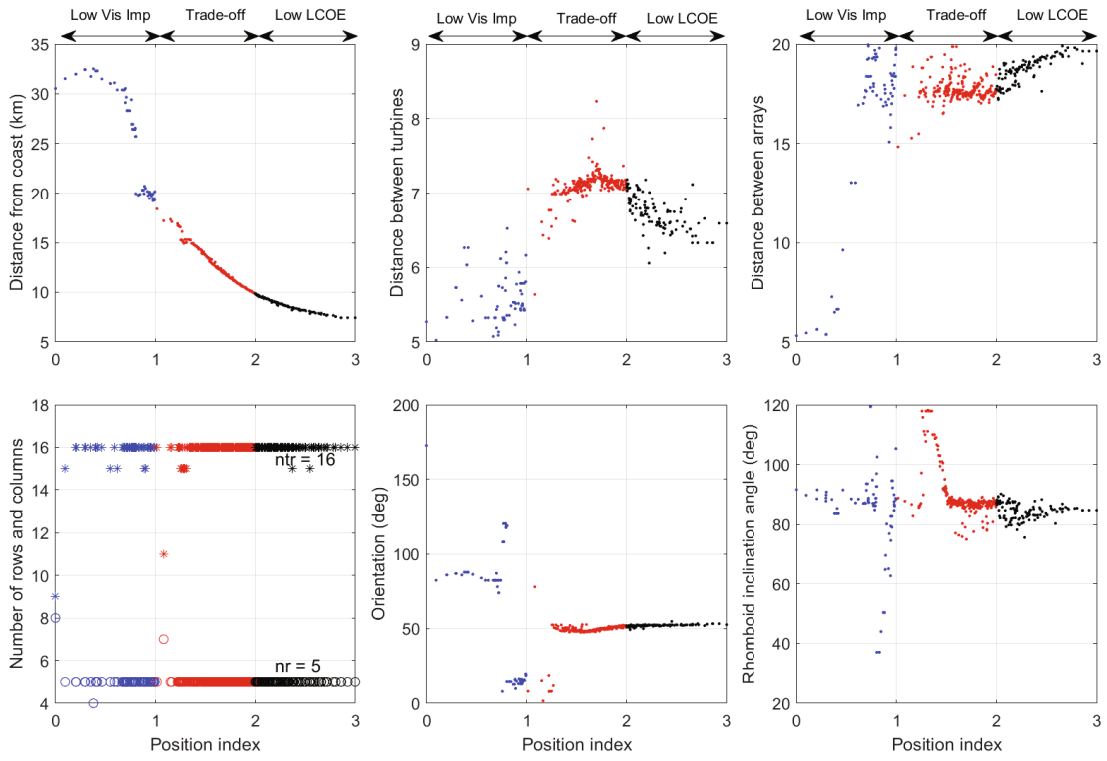

Fig. 13. Distribution of parameters defining the individuals that compose the Pareto front. For each plot, the first third of points (in blue) corresponds to the quasi-horizontal curve with LOW VI; the second one (in red) is a transition zone; and the last third (in black) represents the solutions with low LCOE.

Table 2
Breakdown of costs for three different situations.

	Low LCOE	Transition	Low VI
LCOE (€/MWh)	58.87	60.80	62.85 M€
VI (%)	0.9126%	0.2467%	0.062%
Turbines	80	80	80
Energy yield (GWh)	751.71	757.31	736.54
Turbines (M€)	154.8	154.8	154.8
Foundation (M€)	47.49	52.31	50.48
Elect. Infr. (M€)	53.19	63.31	73.27
Eng. SCADA (M€)	15.2 €	15.2	15.2

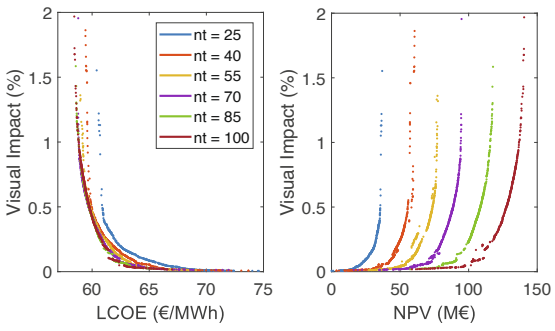

Fig. 14. Non-dominated solutions for six different OWF sizes.

extends by a rectangle of 70 km× 27 km, with irregularly distributed depth curves (see Fig. 11) and a coast outline. They correspond to Horns Rev 1 site, and Wind data as well as the turbine characteristics have been also extracted from this site. Wind data have been obtained from [33] and bathymetric data are provided by GEBCO through the web page of Global Wind Atlas as indicated in https://globalwindatlas.info/about/dataset. Different types of seabed or a concession area delimiting the farm location have not been considered in this work, although a forbidden band parallel to the coast has been included together with the prohibited extraction areas. Other input data, collected in [22,24], are presented in Appendix A, and also published as an Excel file in [23].

These data are required to deduce LCOE from (1). Table A.3 gathers the wind data, and Table A.4, the wind turbine characteristics. Data from Table A.5 are required to select the best MV cable, and together with Table A.6 also necessary to obtain the electrical losses. Table A.7 contains additional data to calculate the yearly net cash flow, once the energy yield has been calculated. Tables A.8 and A.9 are necessary to calculate the initial investment.

3.1. Results for 80 turbine layout

The number of turbines nt is bounded between 76 and 84 (80 ±4). With regard to the search algorithm, the following data applies: population size, 500 individuals; maximum number of generation, 150; offspring size, 508 individuals; crossing probability, 80%; mutation probability, 12% (the inverse of the number of design variables [18]).

As previously indicated, a NSGA-II algorithm was used, following the scheme of Fig. 10.

Fig. 12 shows the set of 500 individuals in four moments of the search process using the NSGA II technique. In the first generations, the individuals of each population are scattered and away from the *optimal* Pareto front. In the last generations, basically from generation 50 on, most of the individuals are non-dominated, and also part of the final Pareto front or are close to it.

An interesting feature of Fig. 12 is the slope of different zones of the

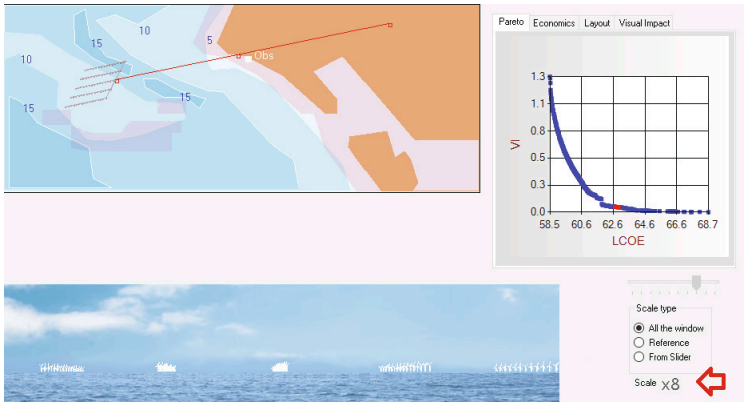

Fig. 15. Non-dominated solution for a middle-distance OWF.

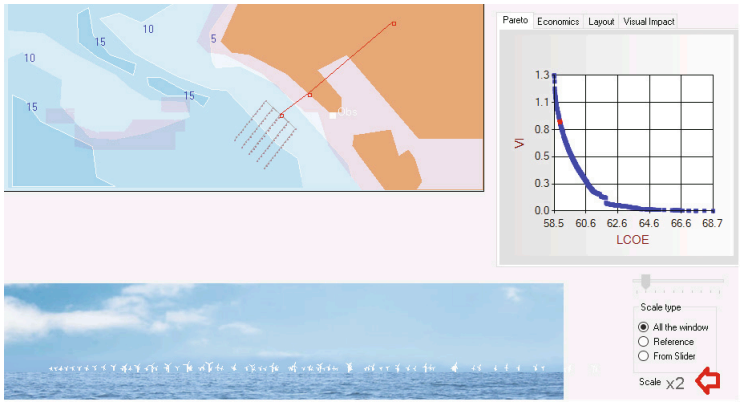

Fig. 16. Non-dominated solution for a close OWF.

Table A.3
Values for probability, and Weibull parameters (scale factor A at 62 m and shape factor WeibK) for every sector.

	N	NNE	NEE	E	EES	ESS	S	SSW	SWW	W	WNN	WNN
freq (%)	3.8	4.3	5.5	8.3	8.7	6.7	8.4	10.5	11.4	12.2	13.9	6.1
$Weib_A$ (m/s)	8.71	9.36	9.29	10.27	10.89	10.49	10.94	11.23	11.93	11.94	12.17	10.31
$Weib_K$	2.08	2.22	2.41	2.37	2.51	2.75	2.61	2.51	2.33	2.35	2.58	2.01

Table A.4
Power and Thrust curve for Vestas V80.

Wind speed (m/s)	1	2	3	4	5	6	7	8	9	10	11	12	13
Power (kW)	0	0	0	66	154	282	460	696	996	1341	1661	1866	1958
Thrust coef	0	0	0	0.818	0.806	0.804	0.81	0.81	0.807	0.793	0.739	0.709	0.409
Wind speed (m/s)	14	15	16	17	18	19	20	21	22	23	24	25	
Power (kW)	1988	1997	1999	2000	2000	2000	2000	2000	2000	2000	2000	2000	
Thrust coef	0.314	0.249	0.202	0.17	0.14	0.119	0.102	0.088	0.077	0.067	0.06	0.05	

Pareto front, indicating regions with very high and very low sensitivity for both objectives. A similar reasoning is presented in [16]. As illustrated, in these two zones each objective reaches a value near the optimum. Between them there is a transition zone, which has been zoomed in. The quasi-horizontal region can be disregarded because it corresponds to solutions where LCOE can be reduced (=improved) without practically deteriorating the *VI*.

Fig. 13 represents the distribution of the parameters that define the solutions. An explanation of these parameters was given in Fig. 2. A selection index (*si*) has been used to distinguish between zones in the decision variable space: $0 \leqslant si \leqslant 1$ for the low VI zone, coloured in blue; $1 < si \leqslant 2$ for the transition zone, in red; and $2 < si \leqslant 3$ for the low LCOE zone, in black. This index is monotonic with respect to both objectives.

From left to right, in the upper row, the represented parameters are: distance to coast, distance (in diameters) between turbines in an array, and distance (in diameters) between arrays. The lower row represents: nr (circles) and ntr (asteriscs); orientation respect to North; and parallelogram inclination angle (equal to 90 deg for rectangular-shape OWFs). The first plot in this lower row shows that, in order to optimize LCOE, the preferred layout consists of five rows, with sixteen

Table A.5
Acquisition cost and characteristics of inner array cables.

Cross area mm^2	Fixed losses W/m	Variable losses W/A^{2}m	I_{max} A	Price €/m
A95	0	7.14E−4	380	128
A150	6	4.35E−4	430	192
A400	24	1.92E−4	680	321
A630	34	1.23E−4	780	481
A800	50	0.86E−4	900	506
B95	0	8.33E−4	260	384
B150	6	5E−4	360	417
B400	8	1.72E−4	640	514
B630	10	1.11E−4	790	535
B800	12	0.86E−4	900	616
Additional cable length for connections: 40 m/turbine				

Table A.6
Acquisition cost of export and HV onshore cable.

			Export cable		Onshore cable	
Voltage (kV)	Section (mm^2)	Var.Loss W/A^{2}m	Capac. (MVA)	Cost (€/m)	Capac. (MVA)	Cost (€/m)
220	500	6E−5	250	843	273	233
220	630	5E−5	273	946	297	266
220	800	4E−5	295	1061	314	299
220	1000	3E−5	314	1214	348	367

Table A.7
Items affecting the yearly cash flow.

Concept	Cost
O&M Costs	15 €/MWh
Increase	5% per year
Surface and insurances	included in O&M
Price of energy *	130 €/MWh
Increase *	0% per year
Availability	95%

* Necessary to calculate NPV of Fig. 14

Table A.8
Non electrical items affecting the investment and decommissioning.

Concept	Cost
Design	95 k€/MW
SCADA	50 k€/turbine
Turbines	
Acquisition	765 k€/MW
Installation	405 k€/MW
Foundations	
Reference price	450 €/MW at 15m depth, Zone 1
Increase	+2% per metre depth +30% for zone 2 +60% for zone 3
Vessels mob demob	430 k€
Decommission	120 k€/MW

Table A.9
Electrical items affecting the investment.

Concept	Cost
Acq. MV cables	see Table A.5
Installation	120 €/m
Acq. export cables	see Table A.6
Installation	170 €/m
Acq. onshore cables	see Table A.6
Inst. onshore cables	400 €/m
Offshore substation	76 k€/MW
Offshore trafo	19 k€/MW
Vessels mob demob	430 k€
Reactive Compens.	128 k€/MVA
Onshore substation	49 k€/MW
Onshore trafo	11 k€/MW
Conn. to grid	200 k€/MW
Shoreline	1.65 M€
OWF Power factor	0.85

turbines each.

The plots show a high dispersion of solutions for low VI ($si \leqslant 1$). As a rule of thumb, the only important concern is to be far enough from the shore. When low LCOE values are required ($si \rightarrow 3$), all of the solutions approximately shares the same layout, although logically increasing the VI when approaching the coast (first plot).

With regard to the transition zone where VI is still reduced, almost constant values for the orientation, turbine distances, and inclination parameters appear to be shared by all solutions on its right. From this point on, the message to the designer is clear: the parameters that define the plant must be those presented in the low LCOE-zone of last five graphs. As deduced from the third and fourth plot, better results are obtained by grouping the turbines in few rows (five) and separating these rows as much as possible. It will depend on the final concession area whether this layout is allowed or not. Any solution defined by these parameters will be a non-dominated one, and it will depend on the social acceptance how close the plant can be to the coast.

If e.g. an OWF is projected in a concession area at 10 km from the coast, the solution corresponds to index = 2 (see first plot of Fig. 13). With this abscissa value, the optimal solution probably consists in an OWF with 7D of distance between turbines in an row, 16D for distance between rows, a layout of 5 rows and 16 turbines per row, orientation = 50 deg and 87 deg for the rhomboid angle.

Table 2 shows three solutions corresponding to *low LCOE*, the *Transition Zone* and *Low VI* zone. The difference in LCOE is due to the cost of the foundations, offshore electrical infrastructure, and the energy yield.

3.2. Results for different farm capacities

The algorithm has been launched considering six different number of turbines. Except for the OWF capacity, input data are kept unvaried. The following values have been considered as reference for nt: 25, 40, 55, 70, 85 and 100. In all cases, a deviation of ±4 turbines is allowed.

Fig. 14 represents the front of non-dominated solutions after NSGA-II algorithm completion. All of the fronts share the same distribution as explained in Fig. 12 for 80 ±4.

The figure at the left represents LCOE and VI. All of the fronts coincide in having a flat part with minimal VI and highly variable economic indicator LCOE. This almost horizontal part, especially the rightmost part, is not interesting because any solution far enough from the coast meets the requirement of low VI. More interesting is the transition zone and the high slope area, where increasing profitability is obtained at the expense of a higher VI.

Except for nt = 25 turbines, there is not a high variation in LCOE when changing the OWF size, which leads to think that economies of scale are not as strong as first assumed. The figure at the right represents NPV and VI, showing a linear variation with the OWF size, as usual in investments where economies of scale are not present.

3.2.1. Photomontages

Figs. 15 and 16 include photo-montages after completing the optimization for 80 ± 4 turbines. They visualize how the OWF would be seen by one of the observers for two of the non-dominated solutions, respectively for medium value of VI and for low value of LCOE- (their respective positions in the Pareto front are represented as red dots in the LCOE-VI plot). Logically, the VI is higher in the second case (please note the scale which is 8 in the first case and 2 in the second one).

4. Discussion

An indicator has been introduced to objectively quantify the visual impact of OWFs. In fact, the visual impact should take into account, not only the intrusion in the visual field calculated in this work, but also more subjective issues such as aesthetics. From a mathematical point of view, VI can be related to the deviation or lack of correlation in the projection of the turbine positions or their height. However, the degree to which these variations increase the visual impact is somewhat subjective and requires an analysis of stimuli outside the scope of this article. Therefore, these terms have not been finally considered in this work in order to take into account exclusively objective issues leading to obtain a human-independent and neutral mathematical indicator.

With regard to the fast method to evaluate the AEP, it is restricted to parallelogram-shaped wind farms such as Horns Rev I, North Hoyle or Belwind (see Fig. 1), and cannot be applied to wind farms with irregular layouts, arbitrary separations between turbines, or with unoccupied positions, either inside or on the edge. In addition, the energy obtained with this method is approximately 0.3% higher than that obtained with the traditional method of calculating the OWF's energy.

Finally, a multi-objective optimization algorithm has been presented. It has been verified that NSGA-II easily adapted to the scenario used, giving satisfactory results of coherence, distribution and density of solutions. Accordingly, NSGA-II has been adopted in this work, although the authors have not tested whether other algorithms provide equally valid results in less time. In addition, the proposed algorithm does not retain a database of discarded solutions, so it is likely that a solution discarded in one generation may appear as part of later offsprings and is evaluated again, with the consequent loss of time. It has been also checked that low density of solutions are obtained for high LCOE and high VI, although in this work, these zones are not of consideration.

This method performs not only the micro-siting (layout) of the OWF, but also its macro-siting (position). However, its location is generally very restricted to a rather small concession area, hence this search functionality in a large geographical area can result of scarce value for wind farm promoters. However, this functionality may be precisely the most useful aspect for governmental institutions when granting concession areas.

5. Conclusions

Mitigating the visual impact of large OWFs is an issue which is becoming increasingly important for the global deployment of this technology. This issue is especially relevant for the development of new offshore projects at relatively close distances from the coastline and in locations of touristic interest.

This paper proposes a new integrated MOOA to maximize the economic performance of OWFs, while minimizing its visual impact, by means of a novel indicator that takes into consideration several realistic aspects for its quantification, such as the visibility in terms of occupancy of the FoV perceived by observers located in different locations of the coast.

Important improvements are obtained through the consideration of regular-shape layouts such as those considered in the vast majority of existing OWFs. By restricting the solutions to UDPSLs, the individual definition is transformed into a set of geometrical parameters. This enables using methods of reduced computational effort in the energy yield assessment function, giving rise to affordable execution times for the optimization of projects composed of high nt in large concession areas. As an example, the energy evaluation for an OWF with 1020 turbines is as low as 5.4 ms.

The algorithm has been successfully validated through the execution of a test case in the location of Horns Rev I, showing the capacity of the MOOA to provide a set of solutions on the Pareto front, which will allow the developer to select the most appropriate configuration according to its needs. The distribution of parameters for the set of non-dominated solutions assists engineers in formulating design guidelines about the optimum distances between turbines, between rows, the optimal orientation, and the inclination angle.

The optimization has been repeated for six different OWF sizes, showing logical displacements to higher LCOE values when moving away from the coast.

This method has two basic applications:

- If there are no constrains in the concession area, or the local administration has to select it, as in the case of Horns-Rev1, Belwind or North Hoyle (see Fig. 1), it directly provides the optimum layout and position, taking into account depth, soil type, and distance of the cables, all maintaining a compromise between adequate profitability and reduced VI. A set of possible positions will be provided to the designer who will choose the nearest one that still maintains an acceptable VI.
- If the concession area is reduced and irregular, or it includes prohibited zones, the designer will fit the turbines within the available space according to the optimum layout provided by the algorithm (distances, orientation and inclination angles as in Fig. 13).

CRediT authorship contribution statement

Angel G. Gonzalez-Rodriguez: Conceptualization, Methodology, Software, Validation, Formal analysis, Investigation, Resources, Data-curation, Writing – original draft, Visualization. **Javier Serrano-Gonzalez:** Formal analysis, Writing – review & editing, Supervision. **Manuel Burgos-Payan:** Methodology, Validation, Investigation, Data-curation, Writing – review & editing, Project administration, Funding-acquisition. **Jesus Riquelme-Santos:** Conceptualization, Methodology, Validation, Writing – review & editing, Funding acquisition.

Declaration of Competing Interest

The authors declare that they have no known competing financial interests or personal relationships that could have appeared to influence the work reported in this paper.

Acknowledgements

This work was partially supported by the Spanish MEC – Ministerio de Economía y Competitividad (Ministry of Economy and Competitiveness), co-funded by the European Commission (ERDF – European Regional Development Fund) under grant ENE2016-77650-R, as well as by the European Commission under grant SI-1778/12/2018. This work was also partially supported by grants US-1265887, Red CYTED 718RT0564 and CER-20191019.

Appendix A. Input data to the algorithm

Table A.3 contains the input data corresponding to the concession. Wind rose has been interpolated to obtain a uniform distribution with resolution of 1deg using the spline interpolation described in [22]. A strip parallel to the coast plus extraction areas are included as forbidden zones. Due to unavailability of confident data, only one type of soil is considered.

The sea depth in the administrative concession is represented as curves of 5 m, 10 m, and 15 m (see Fig. 11).

An only type of turbine will be used. Size and power are given in Table A.4.

According to [22], nominal interest rate (r_i) = 9.4% and *in* f = 1.5% have been used, yielding r = 7.78%.

References

[1] Neubert A, Shah A, Schlez W. Maximum Yield From Symmetrical Wind Farm Layouts, DEWEK 2010, Bremen January (2010) 1–4. http://www.gl-garradhassan.com/assets/downloads/Maximum_Yield_from_Symmetrical_Wind_Farm_Layouts.pdf.

[2] Konstantinidis EI, Kompolias DG, Botsaris PN. Viability analysis of an offshore wind farm in north aegean sea, greece. J Renew Sustain Energy 2014;6(2):023116. https://doi.org/10.1063/1.4871484.

[3] Gonzalez-Rodriguez AG. An indicator to objectively quantify the visual impact of an offshore wind farm. J Renew Sustain Energy 8(2).

[4] Maslov N, Claramunt C, Wang T, Tang T. Method to estimate the visual impact of an offshore wind farm. Appl Energy 2017;204:1422–30.

[5] Serrano González J, Burgos Payán M, Santos JMR, González-Longatt F. A review and recent developments in the optimal wind-turbine micro-siting problem. Renew Sustain Energy Rev 2014;30:133–44. https://doi.org/10.1016/j.rser.2013.09.027.

[6] Renews.biz. Uniform turbine layout touted for NE US offshore wind, Accessed 2 January 2020; 2019. https://renews.biz/56505/.

[7] Guirguis D, Romero DA, Amon CH. Gradient-based multidisciplinary design of wind farms with continuous-variable formulations. Appl Energy 2017;197:279–91. https://doi.org/10.1016/j.apenergy.2017.04.030.

[8] Kirchner-Bossi N, Porté-Agel F. Realistic wind farm layout optimization through genetic algorithms using a Gaussian wake model. Energies 11(12). doi:10.3390/en11123268.

[9] Feng J, Shen WZ. Co-optimization of the shape, orientation and layout of offshore wind farms. J Phys Conf Ser 1618(4). doi:10.1088/1742-6596/1618/4/042023.

[10] Zhang PY, Romero DA, Beck JC, Amon CH. Solving wind farm layout optimization with mixed integer programs and constraint programs. Euro J Comput Optim 2014;2(3):195–219. https://doi.org/10.1007/s13675-014-0024-5.

[11] Zhang PY. Topics in Wind Farm Layout Optimization: Analytical Wake Models, Noise Propagation, and Energy Production; 2013. URL: https://www.academia.edu/3404001/Topics_in_Wind_Farm_Layout_Optimization_Analytical_Wake_Models_Noise_Propagation_and_Energy_Production.

[12] Rodrigues S, Restrepo C, Katsouris G, Teixeira Pinto R, Soleimanzadeh M, Bosman P, Bauer P. A multi-objective optimization framework for offshore wind farm layouts and electric infrastructures. Energies 9(3). doi:10.3390/en9030216.

[13] Tran R, Wu J, Denison C, Ackling T, Wagner M, Neumann F. Fast and effective multi-objective optimisation of wind turbine placement. In Proc. of the 15th Genet. Evol. Comput. Conf., GECCO '13; 2013. pp. 1381–1388. doi:10.1145/2463372.2463541.

[14] Mytilinou V, Kolios AJ. A multi-objective optimisation approach applied to offshore wind farm location selection. J Ocean Eng Mar Energy 2017;3(3):265–84. https://doi.org/10.1007/s40722-017-0092-8.

[15] Rodrigues S, Bauer P, Bosman PA. Multi-objective optimization of wind farm layouts – complexity, constraint handling and scalability. Renew Sustain Energy Rev 2016;65:587–609. https://doi.org/10.1016/j.rser.2016.07.021.

[16] Kwong WY, Zhang PY, Romero D, Moran J, Morgenroth M, Amon C. Wind Farm Layout Optimization Considering Energy Generation and Noise Propagation. In I.D. E.T. Conferences, Computers, I. in Engineering Conference (Eds.), Volume 3: 38th Design Automation Conference, Parts A and B; 2012. pp. 323–332. doi:10.1115/DETC2012-71478.

[17] Herbert-Acero JF, Probst O, Réthoré PE, Larsen GC, Castillo-Villar KK. A review of methodological approaches for the design and optimization of wind farms. Energies 2014;7(11):6930–7016. https://doi.org/10.3390/en7116930.

[18] Deb K, Agrawal S, Pratap A, Meyarivan T. A fast elitist non-dominated sorting genetic algorithm for multi-objective optimization: NSGA-II. In: Schoenauer M, Deb K, Rudolph G, Yao X, Lutton E, Merelo JJ, Schwefel H-P, editors. Parallel Problem Solving from Nature PPSN VI. Berlin, Heidelberg: Springer Berlin Heidelberg; 2000. p. 849–58.

[19] Zitzler E, Thiele L. Multiobjective evolutionary algorithms: a comparative case study and the strength pareto approach. IEEE Trans Evol Comput 1999;3(4):257–71. https://doi.org/10.1109/4235.797969.

[20] Kunkle D. A summary and comparison of MOEA algorithms. Accessed 2 January 2020; 2005. URL: http://www.ccs.neu.edu/home/kunkle/papers/techreports/moeaComparison.pdf.

[21] Wilson D, Rodrigues S, Segura C, Loshchilov I, Hutter F, Buenfil GL, Kheiri A, Keedwell E, Ocampo-Pineda M, Özcan E, Peña SIV, Goldman B, Rionda SB, Hernández-Aguirre A, Veeramachaneni K, Cussat-Blanc S. Evolutionary computation for wind farm layout optimization. Renew Energy 2018;126:681–91. https://doi.org/10.1016/j.renene.2018.03.052.

[22] Gonzalez-Rodriguez AG, Serrano-Gonzalez J, Burgos-Payan M, Riquelme-Santos JM. Realistic optimization of parallelogram-shaped offshore wind farms considering continuously distributed wind resources. Energies 14(10). doi:10.3390/en14102895.

[23] Gonzalez A. Input data for optimization. Mendeley Data 2021;V1. https://doi.org/10.17632/btzfbjh49b.1.

[24] Gonzalez-Rodriguez AG. Review of offshore wind farm cost components. Energy Sustain Dev 2017;37:10–9. https://doi.org/10.1016/j.esd.2016.12.001.

[25] Göçmen T, Laan PVD, Réthoré PE, Diaz AP, Larsen GC, Ott S. Wind turbine wake models developed at the technical university of Denmark: A review. Renew Sustain Energy Rev 2016;60:752–69. https://doi.org/10.1016/j.rser.2016.01.113.

[26] Gonzalez A. Energy production: traditional vs. fast, Mendeley Data, V1 (2021). doi:10.17632/pp7pprrz95.1.

[27] Wagner M, Veeramachaneni K, Frank N, O'Reilly U. Optimizing the layout of 1000 wind turbines. Eur. Wind Energy Assoc. Annu. Event. https://pdfs.semanticscholar.org/4146/95d9ba041143c51a86dfe5f464a0a0291405.pdf.

[28] Gonzalez A. Matlab code for visual impact. Mendeley Data 2021;V1. https://doi.org/10.17632/kz2jzsv3zf.1.

[29] Howard IP, Rogers BJ. Binocular vision and stereopsis. Oxford University Press; 1995. p. 32.

[30] Symonds Group Ltd. Renewable Energy developments: Visual perception versus Photomontage, Countryside Council for Wales, 631st ed.; 2004.

[31] Schiefer U, Pätzold J, Dannheim F, Artes P, Hart W. Part I: Introduction-basic terms. In Conventional Perimetry, With kind permission from Springer Science+Business Media; 2005. pp. 1–23. https://webeye.ophth.uiowa.edu/ips/articles/Conventional-Perimetry-Part-I.pdf.

[32] Wyatt A. Landscape & Visual Assessment Review, Xurban, Stockyard Hill Wind Farm, ABN 18831715013, Accessed 2 February 2020; 2017. https://www.planning.vic.gov.au/_data/assets/pdf_file/0029/9767/West-Wind-energy_EWS_-Allan-Wyatt-30-October-2016.pdf.

[33] Sommer A. Wind resources at Horns Rev. Tech-wise A/S 2002:1–69. URL: https://www.yumpu.com/en/document/view/4469663/wind-resources-at-horns-rev.